Acta Crystallographica Section D
Biological Crystallography
ISSN 0907-4449

The structure of glyceraldehyde 3-phosphate dehydrogenase from *Alcaligenes xylosoxidans* at 1.7 Å resolution

Svetlana V. Antonyuk,[a] Robert R. Eady,[b] Richard W. Strange[a] and S. Samar Hasnain[a]*

[a]Molecular Biophysics Group, CCLRC Daresbury Laboratory, Warrington, Cheshire WA4 4AD, England, and [b]Department of Biological Chemistry, John Innes Centre, Norwich NR4 7HU, England

Correspondence e-mail: s.hasnain@dl.ac.uk

Received 16 September 2002
Accepted 20 February 2003

PDB Reference: glyceraldehyde 3-phosphate dehydrogenase, 1obf, r1obfsf.

The enzyme glyceraldehyde-3-phosphate dehydrogenase (GAPDH) from the Gram-negative denitrifying bacterial species *Alcaligenes xylosoxidans* was purified and crystallized as a contaminant protein during purification of nitrous oxide reductase. This is the first structure of a GAPDH from a denitrifying species. The crystal structure was solved at 1.7 Å resolution by molecular replacement using the structure of GAPDH from *Bacillus stearothermophilus* as a starting model. The quality of the structure enabled the amino-acid sequence of the *A. xylosoxidans* GAPDH to be assigned. The structure is that of the apo-enzyme, lacking the NAD^+ cofactor and with the active-site residue Cys154 oxidized. The global structure of the enzyme has a homotetrameric quaternary structure similar to that observed for its bacterial and eukaryotic counterparts. The essential role of Cys154 in the enzyme activity has been confirmed. In monomer *O* two half-occupancy sulfate ions were found at the active site, which are analogous to the substrate and the 'attacking' phosphate seen in *B. stearothermophilus*. One half-occupancy sulfate ion is also located in the substrate-binding site of monomer *P*.

1. Introduction

Under anaerobic or micro-aerobic conditions, many aerobic species of bacteria can utilize nitrate instead of oxygen as a terminal electron acceptor. In this process, called denitrification, the stepwise reduction of nitrate to dinitrogen *via* nitrite, nitric oxide and nitrous oxide is coupled to the synthesis of ATP formed by oxidative phosphorylation. Denitrifiers are widespread and are among the most successful physiological groups of microorganisms in nature. In ecological terms, denitrification is extremely important since it is the route of formation of almost all atmospheric nitrogen and has both agronomic and environmental impact. It results in the loss of soil nitrogen available for plant growth and generation of the greenhouse gas nitrous oxide (N_2O). *Alcaligenes xylosoxidans* is a Gram-negative denitrifying organism that is common in soil and water. The structure and function of the enzyme and ancillary proteins involved in denitrification are the subject of extensive study in our laboratory. During the isolation of nitrous oxide reductase, a contaminating protein present at significant levels at a late stage of purification was resolved and shown by N-terminal amino-acid analysis to be homologous to D-glyceraldehyde-3-phosphate dehydrogenase (GAPDH; EC 1.1.2.12).

GAPDH is a key enzyme in the glycolytic pathway, since in the presence of inorganic phosphate and NAD^+ it catalyses the reversible oxidative phosphorylation of D-glyceraldehyde-

3-phosphate (GAP) to 1,3-diphosphoglycerate. The enzyme is composed of four chemically identical subunits, each of which binds one molecule of NAD coenzyme. The binding of the coenzyme shows positive or negative cooperativity, depending on the source of the enzyme.

Crystal structures have been solved for GAPDH enzymes isolated from a number of eukaryotic and bacterial species. Two major interests have driven these studies: firstly to establish the structural basis for the extreme thermostability of GAPDH from the archaea and thermophiles and secondly to gain insight to the basis of the cooperativity of cofactor binding. The range of structural studies is wide and in microbial sources includes the mesophiles *Escherichia coli* (Duée *et al.*, 1996) and *Bacillus coagulans* (Griffith *et al.*, 1983), the moderately thermophilic *Bacillus stearothermophilus* (Skarzynski & Wonacott, 1988; Didierjean *et al.*, 1997), the thermophilic *Thermus aquaticus* (Tanner *et al.*, 1996) and the hyperthermophilic *Thermotoga maritima* (Korndörfer *et al.*, 1995). The glycosomal GAPDHs of *Trypanosoma brucei* (Vellieux *et al.*, 1993), *Leishmania mexicana* (Kim *et al.*, 1995) and *Tryponasoma cruzi* (Souza *et al.*, 1998) have been studied. More recently, crystallographic analyses of GAPDHs from *Palinurus versicolor* (Song *et al.*, 1998), *Saccharomyces cerevisiae* (Gilboa *et al.*, 1998), spinach chloroplasts (Sabatino *et al.*, 1999; Fermani *et al.*, 2001), archaeal GAPDH from *Sulfolobus solfataricus* (Fleming *et al.*, 1998; Isupov *et al.*, 1999) and *Methanothermus fervidus* (Charron *et al.*, 1999) have been reported. For three GAPDH structures, *Saccharomyces cerevisiae* (Gilboa *et al.*, 1998), *Thermoproteus tenax* (Brunner *et al.*, 2000) and *Synechococcus* (Nakamura *et al.*, 2001), only preliminary crystallographic analyses are available. All these studies have revealed similar three-dimensional structures. The highest resolution reported so far is 1.8 Å for holo GAPDH from *B. stearothermophilus* and *E. coli*.

Here, we report the crystal structure of GAPDH from *A. xyloxidans* (*Ax*GAPDH) at 1.7 Å resolution, the first for a GAPDH from a denitrifying species, which we show to be essentially in the apo-form lacking the NAD^+ cofactor. The structure exhibits the classical Rossmann fold and has significant structural homology with known GAPDH structures.

2. Materials and methods

2.1. Purification of GAPDH

Protein was initially purified as a contaminant during the purification of *A. xylosoxidans* nitrous oxide reductase. *A. xylosoxidans* was grown anaerobically at 330 K under denitrifying conditions in a 200 l pilot plant fermenter (New Brunswick Scientific) with minimal stirring at 50 rev min^{-1} (Abraham *et al.*, 1993). All purification steps were carried out using 10 m*M* Tris–HCl buffer pH 8.0 (buffer *A*) at room temperature.

Cell paste (500 g) was suspended in 700 ml 50 m*M* Tris–HCl buffer containing small amount of deoxyribonuclease and then disrupted in a pre-cooled Manton–Gaulin homogeniser at 28 MPa. The resulting suspension was then centrifuged at 29 000*g* for 3 h to remove cell debris and unbroken organisms. The supernatant, consisting of a red–brown clear suspension, was then dialysed overnight against buffer *A* (2 × 20 l). The dialysed solution was loaded onto a DE-52 cellulose column (17 × 9 cm) pre-equilibrated with buffer *A*. After the protein solution had been loaded, the column was eluted with a linear gradient of a 50–200 m*M* NaCl (3.4 l total volume) in buffer *A* at a flow rate of 8 ml min^{-1}. GAPDH was eluted as a pink–yellow slightly cloudy band at 90 m*M* NaCl together with nitrous oxide reductase (N_2OR). This fraction was then concentrated to a final volume of 30 ml using an Amicon Centriprep 10 (30 kDa molecular-weight cutoff). It was then loaded onto a gel-filtration column (Sephacryl S-200; 53 × 5 cm) pre-equilibrated with buffer *A* containing 150 m*M* NaCl and eluted at a flow rate of 1.5 ml min^{-1}. A purple band (∼35 ml) showed N_2OR activity. This fraction was diluted with 3.5 *M* ammonium sulfate to an ammonium sulfate concentration of 1.2 *M* and loaded onto a hydrophobic interaction Toyopearl column. Under these conditions, GAPDH present in the sample passed through the column as a single peak, which when analysed by SDS–PAGE gave a single band.

Table 1
Summary of data collection and model refinement statistics.

Data-collection temperature (K)	100
Resolution range† (Å)	50–1.7 (1.76–1.7)
Completeness† (%)	97.6 (90.7)
R_{merge}†‡ (%)	9.9 (35.0)
$I/\sigma(I)$, last shell	2.2
Redundancy	6
Unique reflections	104690
B factor of data from Wilson plot ($Å^2$)	22.7
Unit-cell parameters	a = 89.0, b = 146.6, c = 145.5
Solvent (%)	60.3
Final R_{cryst}§ (%)	16.8
R_{free} (%)	18.9
ESU (Å)	0.08
G factor	0.04
No. of atoms (proteins)	5572 (4995)
No. of water molecules	560
No. of sulfate ions	3
No. of potassium ions	2
Average *B* factor ($Å^2$)	22.3
R.m.s. deviation from ideality¶	
Bond length (Å)	0.012 (0.021)
Planar groups (Å)	0.005 (0.020)
Bond angles (°)	1.497 (1.948)

† Values in parentheses are for the last resolution shell. ‡ $R_{merge} = \sum_h \sum_J |\langle I_h\rangle - I_J(h)| / \sum_h \sum_J I(h)$, where $I(h)$ is the intensity of reflection h, $\sum_h$ is the sum over all reflections and $\sum_J$ is the sum over J measurements of the reflection. § $R_{cryst} = \sum ||F_o| - |F_c|| / \sum |F_o|$. ¶ Values in parentheses are target values.

2.2. N-terminal sequence determination

*Ax*GAPDH (200–300 pmol) was loaded onto an SDS/10% polyacrylamide gel with Tris–glycine as running buffer and then electroblotted onto polyvinylidene difluoride membranes (immobilon_P; Millipore Ltd; Walford, Herts, England) using 10 m*M* CAPS buffer pH 11 as electroblotting buffer. The electroblotted enzyme was then sequenced on an Applied Biosystems Procise Sequencer 490 series.

2.3. Crystallization and data collection

Crystals were grown using the hanging-drop technique. Droplets containing 5 mg ml^{-1} protein, 12% PEG 550, 100 m*M* potassium thiocyanate, 50 m*M* MES buffer pH 6.5 were equilibrated over wells containing 24.5% PEG 550, 200 m*M* potassium thiocyanate, 100 m*M* MES pH 6.5. Crystals grew in 4–7 d to 1.5 mm in length.

Crystallographic data were collected at 100 K using beamline 9.6 at a wavelength of 0.87 Å, giving 626 101 diffraction intensities to 1.7 Å resolution. After processing the data with *HKL*2000 (Otwinowski & Minor, 1997), a total of 104 690 unique reflections were obtained with an $R_{\rm merge}$ of 9.9% on equivalent intensities. Prior to data collection, crystals were transferred for 4 h into a solution containing 25% PEG 400 plus 75% mother liquor. Crystals belong to space group $C222_1$, with unit-cell parameters after cryocooling (100 K) of a = 89.0, b = 146.6, c = 145.5 Å. The asymmetric unit contains two subunits with a molecular mass of 37.2 kDa, giving a solvent content of 59%(v/v).

2.4. Structure solution and refinement

The structure of *Ax*GAPDH was solved by the molecular-replacement method using the program *MOLREP* (Vagin & Teplyakov, 2000) with the *B. stearothermophilus* (*Bs*) holo-GAPDH monomer (PDB code 1gd1) as a starting model. The rotation function shows two peaks at 11.5σ and 11.2σ (the next highest peak was 4.5σ), corresponding to two molecules in the asymmetric unit. Their positioning with the translation function was characterized by a CC of 0.42 and an R factor of 50%. The complete tetramer is generated by the symmetry operation $(-x, y, -z + 1/2)$ of space group $C222_1$.

The model was refined without NCS restraints by the maximum-likelihood method as implemented in *REFMAC*5 (Murshudov *et al.*, 2000) and model building was performed with *O* (Jones, 1978). The quality of the electron-density map was good enough to build a proper model using sequence information for GAPDH from other microbial species together with the 20 N-terminal residues of *Ax*GAPDH determined by Edman degradation. Solvent molecules were added using *ARP* (Lamzin & Wilson, 1993). The water molecules were gradually added to the model and were positioned only when well defined positive peaks were present in both $2F_o - F_c$ and $F_o - F_c$ electron-density maps and when they could form hydrogen bond(s) with either protein atoms or other water molecules. A summary of the crystallographic data-collection statistics and the structure refinement are given in Table 1.

```
Alcaligenes xylosoxidans  TIRVAINGYGRIGRNILRAHYEGGKSHDIEIVAINDLGDPKTNAHLTRY 49
Alcaligenes eutrophus     MTIKVAINGYGRIGRNVLRAHYEGGKRHDLEIVAINDLGNAATNAHLTQY 50
Shewanella oneidensis     MTIRVAINGYGRIGRNVLRALYESEKAYPIKIVAINDLGDASINAHLTKY 50
Pseudomonas aeruginosa    MTIRLAINGFGRIGRNVLRALYTGHYREQLQVVAINDLGDAAVNAHLFQY 50
Neisseria gonorrhoeae     MGIKVAINGYGRIGRQVLRAIYDYQIQDQLQIVAVNASGSLETNAHLTKF 50
Neisseria meningitidis    MGIKVAINGYGRIGRQVLRAIYDYQIQDQLQIVAVNASGSLETNAHLTKF 50
Bradyrhizobium japonicum  MAVRVGINGFGRIGRNVLRAIAESG-RKDIEVVGINDLGPVETNAHLLRF 49
                            ::::.***:*****::***          :::*.:*       **** ::

Alcaligenes xylosoxidans  DTAHGKFPGTVSVNGSYMVVNGDKIRVDANRNPAQLPWGALKVDVVLECT 99
Alcaligenes eutrophus     DTVHGRFPGEVSVDGDAFRVNGDRIRVLAQRNPAELPWGELGVDVVMECT 100
Shewanella oneidensis     DSVHGRFNAKVEHDAEAIYVNGDKILTFQERDPGKLPWNDLQVDVVFECT 100
Pseudomonas aeruginosa    DSVHGHFPGEVEHDAESLRVMGDRIAVSAIRNPAELPWKSLGVDIVLECT 100
Neisseria gonorrhoeae     DTVHGRFEADVSHDGGNLIVNGDKIPFFSTRNPAELPWKELGVDLVMECT 100
Neisseria meningitidis    DTVHGRFEADVSHDGGNLIVNGDKIPFFSTRNPAELPWKELGVDLVMECT 100
Bradyrhizobium japonicum  DSVHGRFPGTVTVDGDSISLGGGKIKVTAERDPSKLPWKDLGVDIALECT 99
                          *:.**:* . *  :.  : : *.:*     *:*.:***  * **:.:***

Alcaligenes xylosoxidans  GFFTTKEKAGAHIKGGAKKVIISAPGGADVDATVVYGVNHGTLKSTDTVI 149
Alcaligenes eutrophus     GLFTSKEKASAHLKGGAKKVIISAPGGKDVDATIVYGVNHGVLKATDTVI 150
Shewanella oneidensis     GIFTSKESVQPHLAAGAKKVIISAPG-KNVDATVVYGVNNNVLTSDMTVI 149
Pseudomonas aeruginosa    GLFTSRDKAAAHLQAGAGKVLISAPG-KDVEATVVYGVNHEVLRASHRIV 149
Neisseria gonorrhoeae     GAFTSKEKAKIHLESGAKKVLISAPGGDDVDATVVYGVNDSVLTADMTVV 150
Neisseria meningitidis    GAFTSKEKAKIHLESGAKKVLISAPGGDDVDATVVYGVNDSVLTADMTVV 150
Bradyrhizobium japonicum  GIFTSKDKASAHLTAGAKRVLVSAPA-DGADATIVYGVNHDTLTKDHLVV 148
                          *:**:::..  *: .** :*::***.  ..:**:*****.  *     ::

Alcaligenes xylosoxidans  SNASCTTNCLAPLVKPLNDKLGLQDGLMTTVHAYTNNQVLTDVYHEDLRR 199
Alcaligenes eutrophus     SNASCTTNCLAPLVKPLHEKLGVVNGLMTTVHSYTNDQVLTDVYHEDLRR 200
Shewanella oneidensis     SNASCTTNCLAPFAKPLNDEIGIESGLMTTIHAYTNDQRLSDVYHTDLRR 199
Pseudomonas aeruginosa    SNASCTTNCLAPVAQVLHRELGIEHGLMTTIHAYTNDQNLSDVYHPDLYR 199
Neisseria gonorrhoeae     SNASCTTNCLSPVAKVLSESVGIVKGAMTTIHALTNDQTVTDVRHKDLRR 200
Neisseria meningitidis    SNASCTTNCLSPVAKVLSESVGIVKGAMTTIHALTNDQTVTDVRHKDLRR 200
Bradyrhizobium japonicum  SNGSCTTNCLAPVAKVLNDLVGIETGFMTTIHAYTGDQPTLDTMHKDLYR 198
                          **.*******:*..: *   :*:  * ***:*: *.:*   *.   ** *

Alcaligenes xylosoxidans  ARSATMSMIPTKTGAAAAVGLVLPELDGKLNGYAIRVPTINVSIVDLSFV 249
Alcaligenes eutrophus     ARSATMSMIPTKTGAAAAVGLVMPELDGRLDGFAVRVPTINVSLVDLSFV 250
Shewanella oneidensis     ARAAALSMIPTKTGAAAAVGLVVPELQGKFDGLAVRVPTVNVSLVDLSFI 249
Pseudomonas aeruginosa    ARSATQSMIPTKTGAAEAVGLVLPELAGKLTGLAVRVPVINVSLVDLTVQ 249
Neisseria gonorrhoeae     ARSGVENMIPTKTGAAKAVGLVLPELKGRLDGLAIRVPTVNVSLVDLSFQ 250
Neisseria meningitidis    ARSGVENMIPTKTGAAKAVGLVLPELKGRLDGLAIRVPTVNVSLVDLSFQ 250
Bradyrhizobium japonicum  GRAAAMSMIPTSTGAAKAIGLVLPELKGKLDGVAIRVPTPNVSVVDLKII 248
                          .*:.. .****.**** *:***:*** *:: * *:***. ***:***..

Alcaligenes xylosoxidans  AKRNTTVEEVNGILK-AASEGELKGILDYNTEPLVSVDYNHDPASSTVDA 298
Alcaligenes eutrophus     AARPTTVEEVNGILK-AAAEGELKGILDYNTAPLVSVDFNHNPASSTFDA 299
Shewanella oneidensis     ASRDTTVEEVNAIIERAASVAPLSEVLAVNKEPLVSIDFNHNAFSSNFDA 299
Pseudomonas aeruginosa    VARDTSVDEVNRLLR-EASEG--SPVLGYNTQPLVSVDFNHDPRSSIFDA 296
Neisseria gonorrhoeae     AARDTTVEEINALMKAASEAGALKGILGYNTLPLVSMDFNHTTEASHFDA 300
Neisseria meningitidis    AARDTTVEEINALMKAASEAGPLKGVLGYNTLPLVSMDFNHTTEASHFDA 300
Bradyrhizobium japonicum  AKRATDVKEINAAMK-RASEQQLKGILGYTNAPNVSIDFNHDPHSSTFHE 297
                          . * * *.*:* :       . :. :*  .. * **:*:** . :* ..

Alcaligenes xylosoxidans        SLTKVS-GRLVKVSSWYDNEWGFSNRMLDTTVALMSAA----- 335
Alcaligenes eutrophus           TLTKVN-GTLVKVSAWYDNEWGFSNRMLDTAVALAHAR----- 336
Shewanella oneidensis           TQTRVN-GRLVKVMAWYDNEWGFSNRMLDNAVALMNAK----- 336
Pseudomonas aeruginosa          NHTKVS-GRLVKAMAWYDNEWGFSNRMLDSALALAAARD---- 334
Neisseria gonorrhoeae           TLTKVVDGNMVKVFAWYDNEWGFSCQMLNTARRMFGLEVRP-- 341
Neisseria meningitidis          TLTKVVDGNMVKVFAWYDNEWGFSCQMLNTARRMFGLEVRPLK 343
Bradyrhizobium japonicum        DQTKVQNGTLVRVMSWYDNEWGFSNRMADTAVAIAKVI----- 335
                                  *:*  * :*:. :********* :* :.: :
```

Figure 1
Multiple alignment of selected known GAPDH sequences from bacterial sources produced using *CLUSTALW* (1.7). Residues conserved on alignment of the top 20 sequences are marked *; non-conserved amino-acid residues are marked with points or colons representing similar or different properties, respectively. The *Ax*GAPDH sequence was built in agreement with this alignment using the electron-density map at 1.7 Å resolution. The residues for which ambiguities remain are underlined and coloured pink.

3. Results and discussion

3.1. Quality of the model

The crystal structure was determined to a final resolution of 1.7 Å with an R factor of 16.6%. All data in the resolution range from 50 Å were used without a σ cutoff, while 5.0% of randomly

distributed reflections were assigned to calculate an R_{free} of 18.9%. The close proximity of R_{free} and R indicates the correctness and high quality of the model.

The final model in the asymmetric unit consists of two subunits, *O* and *P*, and the electron density was sufficiently well defined to allow the positioning of 335 residues in each of the two subunits and 560 water molecules in the asymmetric unit. In addition, the model contains several half-occupancy ligands: three sulfate ions (two in monomer *O* and one in monomer *P*), two potassium ions and one tetraethyleneglycol fragment chain of a PEG molecule.

The dispersion precision indicator (Murshudov *et al.*, 2000) gives an r.m.s error in coordinates of 0.08 Å. The overall *G* factor is 0.04 (*PROCHECK*; Laskowski *et al.*, 1993), which is within the range expected at 1.7 Å resolution. Of the non-glycine residues, 99.7% fall in the most favoured regions of the Ramachandran plot (Ramakrishnan & Ramachandran, 1965); only Val241 (φ = 135, ψ = 90°) lies in the disallowed region. This structural feature is conserved among other GAPDHs (Kim *et al.*, 1995; Vellieux *et al.*, 1993; Skarzynski *et al.*, 1987). The electron density for this residue is good in both subunits and the *B* factors are low. The root-mean-square deviation (r.m.s.d.) of peptide units from planarity is 0.09 Å. The average *B* factor is 23.4 Å^2 for all protein atoms and about 30 Å^2 for each of the sulfate ions, potassium ions and PEG-molecule fragments.

Approximately 23.5% of the amino-acid residues are in the α-helical conformation, 27.7% in β-sheets and 4.5% in 3_{10}-helices. During refinement, each subunit was treated independently without imposing NCS fold-symmetry restraints. The r.m.s.d. between C$^\alpha$ positions in the two subunits is 0.29 Å. In the last stages of the refinement, H atoms were placed in positions calculated according to geometry criteria.

3.2. Sequence identification for *Ax*GAPDH

The amino-acid sequences of GAPDHs from 376 (63 bacterial) species have been determined and show sequence identities ranging from 18 to 85%. In the case of *Ax*GAPDH, no sequence information was available; therefore, the N-terminal sequence of the first 20 residues was determined by N-terminal protein sequencing. A BLAST (Altschul *et al.*, 1990) search showed this portion of the sequence to have high homology (up to 89%) with a number of GAPDH sequences from microbial species (Fig. 1). The *B. stearothermophilus* holo-GAPDH monomer was taken as a starting model for building the 'X-ray sequence' of *Ax*GAPDH using the 1.7 Å resolution electron density. During refinement and model rebuilding, it was possible to locate 335 amino-acid residues per subunit. A large number of iterative cycles of model building and refinement were performed with the $2F_o - F_c$ electron-density map calculated using zero side-chain occupancy for the non-conserved residues. The electron-density maps revealed differences in the *Ax*GAPDH sequence in comparison with *Bs*GAPDH. All residues with aromatic side chains were clearly visible in the original map and residues situated in the inner part of the molecule could easily be defined. For example, the density at residue 56 was clearly that corresponding to a Phe, not a Leu as in the case of *BsGAPDH* (Fig. 2). This residue is also a Phe in all other bacterial sequences (Fig. 1). Alignment of the *Ax*GAPDH sequence derived from the built structure compared with the 20 top-scoring GAPDH sequences allowed us to check that conserved residues were positioned and assigned correctly. Where residues could not be unambiguously determined from the electron density, *i.e.* Asn or Asp, Gln or Glu and Val or Thr, the most frequently assigned amino acid from the 'top-scoring' sequences was selected. Identities were also assigned based on their hydrogen-bonding patterns with neighbouring residues and water molecules. There is still ambiguity remaining in residues Asp39, Asn63, Val76, Gln84, Thr141, Asn186 and Asn230 (Fig. 1) situated on the surface of the molecule with high solvent accessibility and high temperature factors.

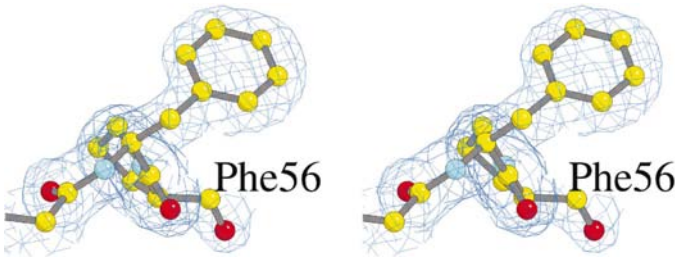

Figure 2
The $2F_o - F_c$ electron-density map at the 3σ level clearly shows Phe instead of Leu as in the starting model.

3.3. Structure description and comparison with GAPDH from *B. stearothermophilus*

Since the three-dimensional structures of prokaryotic, eukaryotic and archaeal GAPDHs are highly conserved, the structure of *Ax*GAPDH will be compared with the *B. stearothermophilus* enzyme, one of the two for which the highest resolution structure of 1.8 Å is available (Skarzynski & Wonacott, 1988; Duée *et al.*, 1996).

The *Ax*GAPDH subunit monomer has two folding domains, the nucleotide (NAD^+) binding domain and the catalytic (GAP-binding) domain. The NAD^+-binding domain, consisting of residues 1–152 and 314–335, is formed by a six-stranded parallel β-sheet with helices on both sides of the sheet and may be represented by a highly conserved double β–α–β–α–β motif fold (Lesk, 1995). The α/β fold of the catalytic domain (residues 153–313) is more variable, mainly consisting of antiparallel β-sheet. Superposition of the *Ax*GAPDH and *Bs*GAPDH amino-acid sequences and dentification of the secondary-structure elements is shown in Fig. 3(*a*).

The *Ax*GAPDH and *Bs*GAPDH subunits were superimposed using β-sheets from both domains. The least-squares algorithm implemented in the program *O* was then used to obtain the best fit of the C$^\alpha$ atoms to give an r.m.s.d. of 1.02 Å (maximum of 4.3 Å) for the 332 matching atoms of the 335 atoms of the sequence. The catalytic domains of the two

enzymes superimpose better than the whole subunits, with an r.m.s.d. of 0.48 Å. The catalytic domains of holo *Bs*GAPDH and *Ax*GAPDH are rotated by about 5° (Skarzynski & Wonacott, 1988). The NAD-binding domains show more structural difference than the catalytic domains and can be superimposed with an r.m.s.d. of 1.09 Å for matching C^{α} atoms (Fig. 3*b*). No additional structural elements were found in *Ax*GAPDH, but there are three insertion residues, Gly23, Gly24 and Lys25, which elongate the first α-helix. As in the other known GAPDHs, there are no salt bridges between the catalytic and NAD-binding domains.

```
                SSSSSS  HHHHHHHHHHHHHH     SSSSSSS   HHHHHHHHHH
A.xylosoxidans   TIRVAINGYGRIGRNILRAHYEGGKSHDIEIVAINDLGDPKTNAHLTRYDTAHGKFPGT 59
B.stearotherm.  -AVKVGINGFGRIGRNVFRAALK---NPDIEVVAVNDLTDANTLAHLLKYDSVHGRLDAE 56
                 SSSSSSS HHHHHHHHHHHH      SSSSSSSSS   HHHHHHHHHH   SSS  S
                  ::.***:***** : *          : :**:*   .  . *** ::*:.* :: .

               SSSS  SSSS  SSSSSS   GGGGG        SSSS      HHHHHHHHHH   SS
A.xylosoxidans VSVNGSYMVVNGDKIRVDANRNPAQLPWGALKVDVVLECTGFFTTKEKAGAHIKGGAKKV 119
B.stearotherm. VSVNGNNLVVNGKEIIVKAERDPENLAWGEIGVDIVVESTGRFTKREDAAKHLEAGAKKV 116
               SSSS  SSSSS SSSSSS   GGGGGGGGGG   SSSSSS    HHHHHHHHHH   SS
               *.     : * *..* . :  :* :*.*    **.* *.** * .: .*  *...** **

               SS          SS     GGGGG      SSS    HHHHHHHHHHHHHHH SSSSSSSS
A.xylosoxidans IISAPGGADVDATVVYGVNHGTLKS-TDTVISNASCTTNCLAPLVKPLNDKLGLQNGLMT 178
B.stearotherm. IISAPA-KNEDITIVMGVNQDKYDPKAHHVISNASCTTNCLAPFAKVLHEQFGIVRGMMT 175
               SSS         SSS    GGGGG     SSSSS HHHHHHHHHHHHHHHHHHHSSSSSSS
               :*:**.  . : *:* * *.    .    ::* ******.::*..: *  ..*:  * :*

               SSSS                          SSS      HHHHHHGGGG  SSSSSSSS
A.xylosoxidans TVHAYTNNQVLTDVYHEDLRRARSATMSMIPTKTGAAAAVGLVLPELDGKLNGYAIRVPT 238
B.stearotherm. TVHSYTNDQRILDLPHKDLRRARAAAESIIPTTTGAAKAVALVLPELKGKLNGMAMRVPT 235
               SSSS                          SSSSS  GGGGGGGGGGGG SSSSSSSSS
               *:*: ****   *  * ** ***:.. .:***.**** **.**:**: .:* * *:***

                  SSSSSSSSS    HHHHHHHHHHHHHHH     SSSS    GGGGGG     SSSS
A.xylosoxidans INVSIVDLSFVAKRNTTVEEVNGILKAASEGELKGILDYNTEPLVSVDYNHDPASSTVD 297
B.stearotherm. PNVSVVDLVAELEKEVTVEEVNAALKAAAEGELKGILAYSEEPLVSRDYNGSTVSSTID 294
                  SSSSSSSSSS   HHHHHHHHHHHHHH    SSSSS    GGGGGG     SSSS
               : *:.**     : .:::*:*  :: *:: *    :: *.  *:** *    . :. .*

                GGGSSS   SSSSSSSS  HHHHHHHHHHHHHHHHH
A.xylosoxidans ASLTKVS-GRLVKVSSWYDNEWGFSNRMLDTTVALMSAA----- 335
B.stearotherm. ALSTMVIDGKMVKVVSWYDNETGYSHRVVDLAAYIASKGL---- 334
               SSSSSSS  SSSSSSSSS  HHHHHHHHHHHHHHHHHH
               *  * *  * ::*. :***** *:* :: :    :

A.xylosoxidans - Alcaligenes xylosoxidans
B.stearotherm  - Bacillus stearothermophilus     Identities = 186/334 (55%)
```

(*a*)

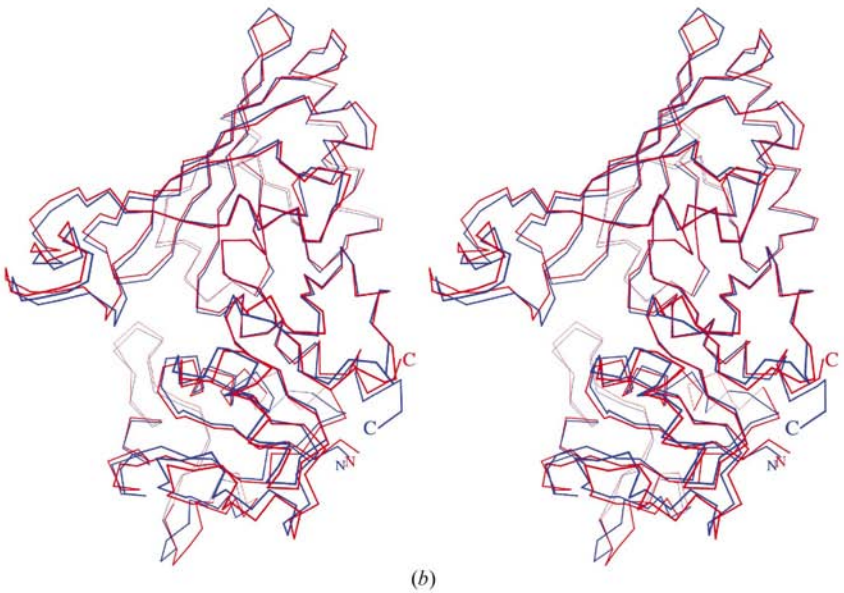

(*b*)

Figure 3
(*a*) The amino-acid sequence of the native *Ax*GAPDH enzyme (top) is shown aligned with the *Bs*GAPDH enzyme sequence (bottom) on the basis of structural superposition. Amino-acid sequence and numbering of residues for *Bs*GAPDH are from the X-ray structure (PDB code 1gd1). α-Helices, β-strands and 3_{10}-helices are indicated by the labels H, S and G, respectively. Conserved residues are shown in red. (*b*) Stereo plot of C^{α} traces of one subunit of *Ax*GAPDH and *Bs*GAPDH superimposed using the program *O* (Jones, 1978). The subunit C^{α} trace of *Bs*GAPDH is shown in blue.

3.4. Tetrameric structure

The dimer *OP* generates the tetramer *OPRQ* using a crystallographic twofold axis coincident with the molecular axis *P*. The relative positions of subunits in the *Ax*GAPDH tetramer are similar to those in the *Bs*GAPDH tetramer. The *Ax*GAPDH tetramer is 75 × 85 × 91 Å in size, with a solvent-accessible surface area of 38 564 Å^2, calculated according to the method proposed by Lee & Richards (1971). As in all dehydrogenases, a large part of the monomer surface (∼15 000 Å^2) is hidden deep within the tetramer because of the S-loop region at the core of the structure. The S-loop of subunit *O* in *Ax*GAPDH interacts with units *P* and *Q*, while in *Bs*GAPDH it interacts with subunits *R* and *P*. The interface between the *P* and *O* subunits is the largest (2245 Å^2) in the structure. 26 strong interactions are formed across this interface, including six salt bridges (Table 2). This interface also contains a large hydrophobic cluster, where five residues (Val180, Pro209, Ile234, Val236, Ile243) of one subunit interact with their counterparts in the other subunit. The *O*–*R* interface area is 1905 Å^2 and includes 19 hydrogen bonds. The *O*–*Q* interface area is the smallest (905 Å^2) and involves only five hydrogen bonds and one salt bridge. Despite the differences in crystalline environment, the two subunits are structurally very similar and are related by twofold molecular symmetry. The subunits were superimposed using all C^{α} atoms, which gives an r.m.s.d. of 0.30 Å.

3.5. Active site

The electron density provides no evidence of co-enzyme at the position of the NAD$^+$-binding site, showing the structure to be essentially that of apo-enzyme. The electron density in the active site clearly reveals the presence of two sulfate ions (average *B* factors are 30 Å^2 with occupancy 0.5, similar to those seen in the

enzyme from *B. stearothermophilus*). There were no sulfate ions present in the crystallization media, so it appears that *Ax*GAPDH binds the sulfate ions during the purification process. The first sulfate occupying the position of the C3 phosphate of the substrate (site P_s; Moras *et al.*, 1975) is located close to the S-loop and makes hydrogen bonds with the side-chain O atom of Thr184, the guanidinium groups of Arg199 and Arg235 and with two molecules of water. The orientation of the sulfate O atoms is clearly defined in the electron density. The guanidinium groups of Arg199 and Arg235 are equivalent to the guanidinium groups of Arg195 and Arg231 in *Bs*GAPDH (Fig. 4*a*).

The second sulfate ion in the inorganic site (P_i) is bound as Sul339, as seen in the *Bs*GAPDH structure. It forms hydrogen bonds to side-chain atoms of the conserved residues Ser153 and Thr212 and the main-chain N atom of Gly213 and also to four surrounding water molecules. Two of these waters in turn form hydrogen bonds to the side chains of the neighbouring conserved residues Ser155 and His181 (Fig. 4*b*).

The conserved residues Cys154 and His181, which are directly involved in catalysis, are both well defined. There is additional electron density associated with the S atom of Cys153. Analysis of this density indicated that the side chain of Cys154 in both subunits has undergone full oxidation and three fully occupied O atoms are bound to the S atom (Fig. 4*c*). It is highly probable that oxidation occurred during purification of the protein, since as it was purified as a contaminant and no preventive measures were taken to avoid oxidation of the active cysteine residue. Nevertheless, comparison with other GAPDH structures shows that oxidation does not affect the position of the S atom or other neighbouring protein residues.

His181 ND1 is hydrogen bonded to the carboxyl O atom of Ala182, fixing the plane of the histidine ring, while the other N atom acts as proton acceptor during catalysis. In the present structure, this nitrogen is hydrogen bonded to one of Cys154 O atoms. The distance from the S atom of Cys154 to this nitrogen is 3.9 Å. This region of the active site is arranged very similarly in all other GAPDHs, suggesting the importance of the configuration and supporting the view that a lock-and-key mechanism is operative.

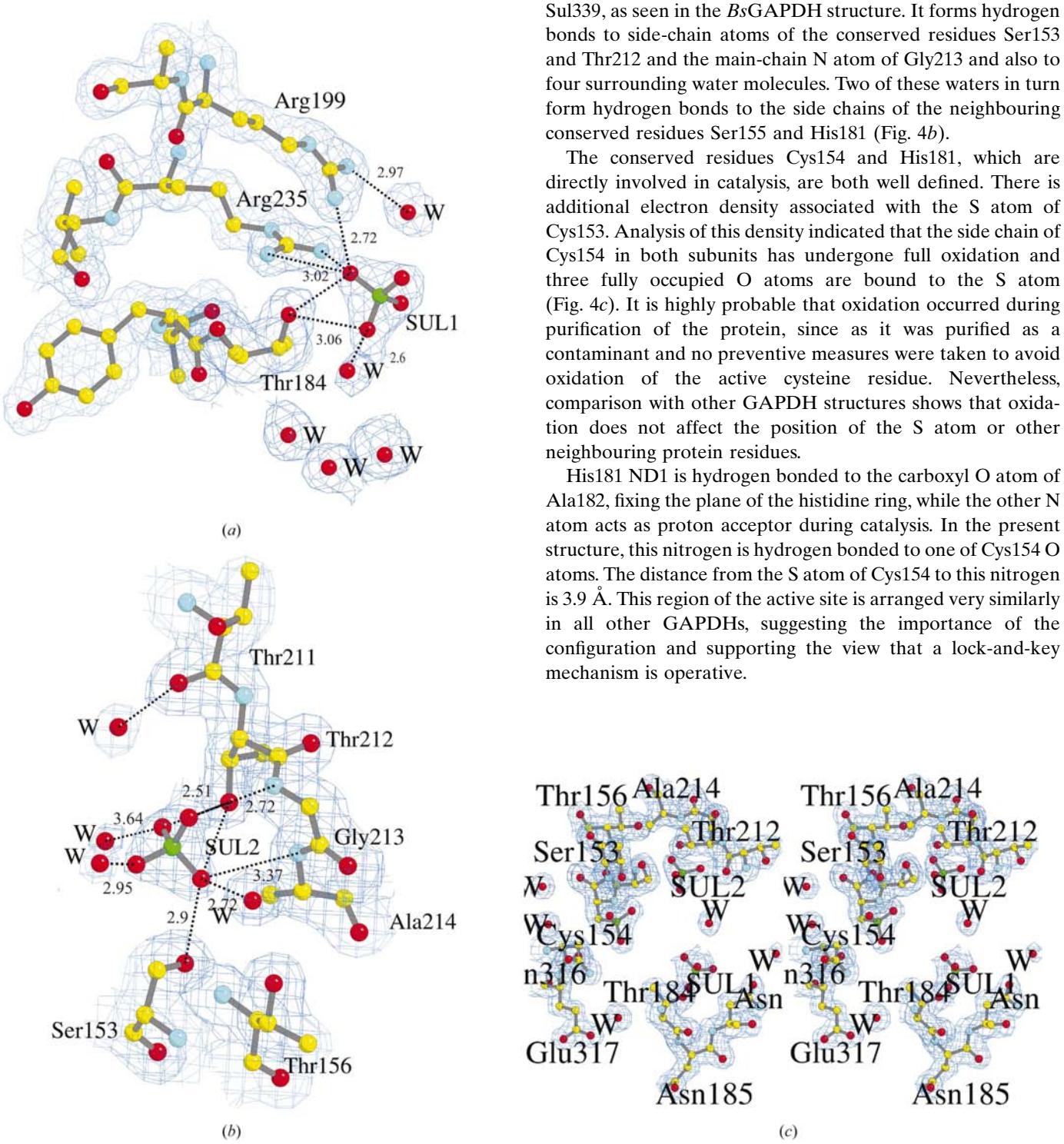

Figure 4
$2F_o - F_c$ electron-density map around the active site and sulfate ions (contoured at 1σ). (*a*) P_s binding site; (*b*) P_i binding site; (*c*) overview of the active site. Important hydrogen bonds are shown as red dotted lines (lengths in Å).

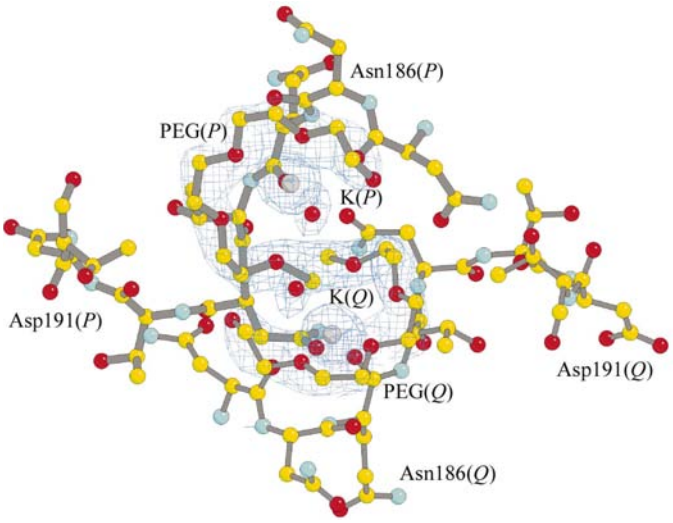

Figure 5
$2F_o - F_c$ electron-density map contoured at 1σ around the PEG molecule and potassium ions near the S-loop area at the dimer–dimer interface.

3.6. PEG-binding site

The *Ax*GAPDH structure differs from all other GAPDHs in the S-loop region. It is probable that this difference is primarily a consequence of the binding of a tetraethyleneglycol fragment of a PEG molecule in the axis region of the tetramer core on the twofold axis in the *P* and *Q* molecules. The PEG fragment has an S shape and surrounds two metal ions (probably potassium ions), coordinating to carboxyl O atoms of S-loop residues Asn185, Asn186 and Gln187. Although the atoms of the PEG molecule have an occupancy of 0.5, they have very clearly defined electron density, with the O atoms coordinating to the potassium ions from one side and the carboxyl oxygen of Tyr193 and a water molecule forming hydrogen bonds from the other side (Fig. 5). The electron density of PEG is better defined in the *P* subunit. It was difficult to model ethyleneglycol fragments in molecule *O*. Electron density appearing to be similar to two ethyleneglycol fragments was modelled as chain of waters with half-occupancy.

4. Concluding remarks

The tetrameric structure of the first GAPDH isolated from a denitrifying bacterium has a molecular architecture that closely resembles those determined from a variety of sources. The structure reported here represents the highest resolution for any known GAPDH. The tetrameric structure of *Ax*GAPDH is formed from two dimers and involves eight hydrogen bonds. The catalytic domain in *Ax*GAPDH is rotated by about 1° relative to apo *Bs*GAPDH and 5° relative to holo *Bs*GAPDH. Similar differences are known between apo and holo forms of other GAPDHs. Two sulfate ions are located in the monomer *O*, one in the position of the substrate phosphate group (GAP) and the other in the inorganic phosphate-ion site. The position of these sulfate ions is in agreement with those in the apo and holo structures of *Bs*GAPDH. The apo form of *Ax*GAPDH has weak ion–protein interactions at both phosphate-binding sites, in

Table 2
Selected salt-bridge (s.b.) and hydrogen-bond-type interactions across the *O*–*P*, *O*–*R* and *O*–*Q* interfaces.

(*a*) *O*–*P* interface.

Monomer *O*	Monomer *P*	Distance (Å)
Asn174 ND2	Ser304 OGx	3.01
Thr178 OG1	Asp245 OD2	2.68
Thr178 OG1	Lys309 NZ	3.14
Arg198 NH1	Leu282 O	2.8
Arg198 NH1	Asp297 OD2	2.9 (s.b.)
Arg198 NH2	Asp297 OD1	3.24
Arg201 NH1	Asp286 OD1	2.80 (s.b.)
Arg201 NH2	Asp286 OD2	2.83 (s.b.)
Ser206 OG	Val285 N	3.22
Met207 N	Ser284 OG	2.91
Tyr232 OH	Asn245 OD2	2.94
Ser304 OG	Asn174 ND2	315
Ser304 OG	Ser311 OG	2.76
Asp245 OD2	Tyr232 OH	2.94
Asp245 OD2	Thr178 OG1	2.73
Leu282 O	Arg198 NH1	2.89
Ser284 N	Met207 O	3.20
Ser284 OG	Met207 N	2.92
Val285 N	Ser206 OG	3.13
Asp286 OD1	Arg201 NH1	2.84 (s.b.)
Asp286 OD2	Arg201 NH2	2.88 (s.b.)
Asp297 OD2	Arg198 NH1	2.90 (s.b.)
Ser304 O	Asn174 ND2	3.26
Ser304 OG	Asn174 ND2	2.96
Lys309 NZ	Thr178 OG1	3.19
Ser311 OG	Tyr232 OH	2.99

(*b*) *O*–*Q* interface.

Monomer *O*	Monomer *Q*	
Lys55 NZ	Asp286 O	2.70
Lys113 NZ	Asp130 OD1	2.81 (s.b.)
Asp128 O	Lys113 NZ	2.91
Asp130 OD1	Lys113 NZ	3.51
Glu280 OE1	Tyr49 OH	2.80
Asp286 O	Lyz55 NZ	2.86

(*c*) *O*–*R* interface.

Monomer *O*	Monomer *R*	
Arg11 NH1	Asp191 O	2.97
Arg14 NH2	Asp191 O	3.09
Asp39 N	Tyr193 OH	3.07
Tyr49 OH	Gln280 NE2	3.12
Asp50 OD2	Asp191 OD2	3.22
Thr51 N	Asp191 OD2	2.91
	Asp191 OD1	2.74
Tyr183 OH	Thr204 OG1	2.76
Asn185 OD1	Thr190 N	3.22
Asn185 ND2	Thr190 O	2.91
Thr190 N	Asn185 OD1	3.22
Thr190 O	Asn185 ND2	2.91
Asp191 O	Arg11 NH1	2.97
Asp191 O	Arg14 NH2	3.09
Asp191 OD1	Thr51 OG1	2.74
Asp191 OD2	Asp50 OD2	3.22
Asp191 OD2	Thr51 N	2.97
Tyr193 OH	Asp39 N	3.07
Thr204 OG1	Tyr183 OH	2.76

agreement with the lower occupancies of sulfate ions in apo *Bs*GAPDH structure compared with its holoenzyme form.

We would like to thank Svetlana Sedelnikova for her help with protein purification. We also acknowledge support from CCLRC and BBSRC.

References

Abraham, Z. H. L., Lowe, D. J. & Smith, B. E. (1993). *Biochem. J.* **259**, 587–593.
Altschul, S. F., Gish, W., Miller, W., Myers, E. W. & Lipman, D. J. (1990). *J. Mol. Biol.* **215**, 403–410.
Brunner, N. A., Lang, D. A., Wilmanns, M. & Hensel, R. (2000). *Acta Cryst.* D**56**, 89–91.
Charron, C., Talfournier, F., Isupov, M. N., Branlant, G., Littlechild, J. A., Vitoux, B. & Aubry, A. (1999). *Acta Cryst.* D**55**, 1353–1355.
Didierjean, C., Rahuel-Clermont, S., Vitoux, B., Dideberg, O., Branlant, G. & Aubry, A. (1997). *J. Mol. Biol.* **268**, 739–759.
Duée, E., Olivier-Deyris, L., Fanchon, E., Corbier, C., Branlant, G. & Dideberg, O. (1996). *J. Mol. Biol.* **257**, 814–838.
Fermani, S., Ripamonti, A., Sabatino, P., Zanotti, G., Scagliarini, S., Sparla, F., Trost, P. & Pupillo, P. (2001). *J. Mol. Biol.* **314**, 527–547.
Fleming, T. M., Jones, C. E., Piper, P. W., Cowan, D. A., Isupov, M. N. & Littlechild, J. A. (1998). *Acta Cryst.* D**54**, 671–674.
Gilboa, R., Bauer, A. J. & Shoham, G. (1998). *Acta Cryst.* D**54**, 1467–1470.
Griffith, J. B., Lee, B., Murdock, A. L. & Amelunxen, R. E. (1983). *J. Mol. Biol.* **169**, 963–974.
Isupov, M. N., Fleming, T. M., Dalby, A. R., Crowhurst, G. S., Bourne, P. C. & Littlechild, J. A. (1999). *J. Mol. Biol.* **291**, 651–660.
Jones, T. A. (1978). *J. Appl. Cryst.* **11**, 268–272.
Kim, H., Feil, I. K., Verlinde, C. L. M. J., Petra, P. H. & Hol, W. G. J. (1995). *Biochemistry*, **34**, 14975–14986.
Korndörfer, I., Steipe, B., Huber, R., Tomschy, A. & Jaenicke, R. (1995). *J. Mol. Biol.* **246**, 511–521.
Lamzin, V. S. & Wilson, K. S. (1993). *Acta Cryst.* D**49**, 129–147.
Laskowski, R. A., MacArthur, M. W., Moss, D. S. & Thornton, J. M. (1993). *J. Appl. Cryst.* **26**, 283–291.
Lee, B. & Richards, F. M. (1971). *J. Mol. Biol.* **55**, 379–400.
Lesk, A. M. (1995). *Curr. Opin. Struct. Biol.* **5**, 775–783.
Moras, D., Olsen, K. W., Sabesan, M. N., Buehner, M., Ford, G. C. & Rossmann, M. G. (1975). *J. Biol. Chem.* **250**, 9137–9162.
Murshudov, G. N., Vagin, A. A. & Dodson, E. J. (2000). *Acta Cryst.* D**53**, 240–255.
Nakamura, Y., Tada, T., Wada, K., Kinoshita, T., Tamoi, M., Shigeoka, S. & Nishimura, K. (2001). *Acta Cryst.* D**57**, 879–881.
Otwinowski, Z. & Minor, W. (1997). *Methods Enzymol.* **276**, 307–326.
Ramakrishnan, C. & Ramachandran, G. N. (1965). *Biophys. J.* **5**, 909–933.
Sabatino, P., Fermani, S., Ripamonti, A., Casseta, A., Scagliarini, S. & Trost, P. (1999). *Acta Cryst.* D**55**, 566–567.
Skarzynski, T., Moody, P. C. E. & Wonacott, J. A. (1987). *J. Mol. Biol.* **193**, 171–187.
Skarzynski, T. & Wonacott, A. J. (1988). *J. Mol. Biol.* **203**, 1097–1118.
Song, S., Li, J. & Lin, Z. (1998). *Acta Cryst.* D**54**, 558–569.
Souza, D. H. F., Garratt, R. C., Araujo, A. P. U., Guimaraes, B. G., Jesus, W. P. D., Michels, P. A. M., Hannaert, V. & Oliva, G. (1998). *FEBS Lett.* **424**, 131–135.
Tanner, J. J., Hecht, R. M. & Krause, K. L. (1996). *Biochemistry*, **35**, 2597–2609.
Vagin, A. & Teplyakov, A. (2000). *Acta Cryst.* D**56**, 1622–1624.
Vellieux, F. M. D., Hajdu, J., Verlinde, C. L. M. J., Groendijk, H., Read, R. J., Greenhough, T. J., Campbell, J. W., Kalk, K. H., Littlechild, J. A., Watson, H. C. & Hol, W. G. J. (1993). *Proc. Natl Acad. Sci. USA*, **90**, 2355–2359.